

# 1D Temperature Measurements by Air **REMPI Thermometry (ART)**

Walker McCord<sup>1</sup>, Alek Clark<sup>2</sup>, and Zhili Zhang<sup>3,\*</sup>

Dept. of Mechanical, Aerospace, and Biomedical Engineering, University of Tennessee, Knoxville, TN 37996, USA

In this work, a detailed calibration study is performed to establish non-intrusive 1D rotational temperature measurements based on Air Resonance enhanced multiphoton ionization Thermometry (ART) as a technique. First by using coherent microwave scattering (Radar) from REMPI (Resonance Enhanced Multi-Photon Ionization), analysis of the rotational line strengths of the 2-photon transition of molecular oxygen  $C^3\Pi$  (v=2)  $\leftarrow X^3\Sigma$ (v'=0) have been conducted. Experimentally found hyperfine structures of the O2 rotational branches are then used to derive a relationship that is temperature sensitive. The structures (peaks) that exhibit high temperature sensitivity are selectively excited through a frequencydoubled dye laser. Electron-avalanche ionization of N2 results in the fluorescence emissions from the first negative bands of  $N_2$  near 390, 425, and 430nm, which are captured as a 1D line by a gated high-speed ICCD camera. Post processing of the fluorescence images yields a 1D thermometry line for the local rotational temperature of  $O_2$ . The technique thus provides the means to quantitatively measure the 1D temperature of the unseeded air, which could be used in high-speed wind tunnels and other ground test facilities.

## I. Nomenclature

the rotational quantum number

total angular momentum except the spin

Polarization Coefficient Laser Beam Intensity **Boltzmann Constant** Ground State Energy

Total number of O<sub>2</sub> molecules two-photon transition line strength

the excitation wavelengths for molecular oxygen

## II. Introduction

A renewed growth in hypersonic and high-supersonic research and development has resulted in increased desire for flow characterization techniques that can serve as a means of CFD validation tools. The facilities built that employ these techniques provide high-speed flow conditions that aim to accurately simulate various aspects of in-flight flow conditions; at such speeds the use of probes is detrimental as they induce perturbations of sufficient strength that change the phenomena and invalidate most measurements taken in the downstream region of interest. This has led to a renaissance in non-intrusive optical technique that do not induce perturbations of sufficient strength and leave flow

<sup>&</sup>lt;sup>1</sup> Graduate Student, Dept. of Mechanical, Aerospace, and Biomedical Engineering, University of Tennessee, AIAA student member.

<sup>&</sup>lt;sup>2</sup> Graduate Student, Dept. of Mechanical, Aerospace, and Biomedical Engineering, University of Tennessee, AIAA

<sup>&</sup>lt;sup>3</sup> Professor, Dept. of Mechanical, Aerospace, and Biomedical Engineering, University of Tennessee, AIAA Associate Fellow.

chemistry unaffected. One of the key design parameters for test beds is thermal protection as the thermal gradients present in the boundary layer becomes extremely important as surface heating dramatically increases as a direct result of increased skin-friction from reduced boundary layer heights. The current techniques that exist for optical thermometry in low pressure, non-heated flows are Planar-Laser Induced Fluorescence (PLIF), Coherent Anti-Stokes Raman Spectroscopy (CARS), and Tunable-diode laser absorption spectroscopy (TDLAS) [1-3]. PLIF has to employ the use of tracer molecules such as Nitric Oxide, Hydroxide, or an aromatic molecule, which can negatively impact the flow chemistry resulting in nonreal flow features and altered flow chemistry [1, 3-5]. CARS is a non-intrusive technique that does not require seeding of the flow for thermal measurements in low-enthalpy, high-speed environments [6, 7]. However, CARS is susceptible to misalignment in high-noise environments typically found in wind tunnel facilities and its accuracy decreases in low enthalpy flow fields as the rotational structure used for spectrum fitting diminishes as population distributions trend towards the ground-state [2]. Furthermore, CARS is limited to point measurements at low pressure conditions, thus rendering it inadequate to fully characterize the dynamic thermal gradients present in boundary layers [2].

The proposed technique builds upon advances in Radar Resonate Enhanced Multi-Photon Ionization (Radar-REMPI), which has been recently demonstrated to have the capability to achieve high spatial and temporal resolution measurements of concentration profiles and species-specific rotational temperatures in combustion and air-discharge environments [8-10]. ART differentiates from Radar REMPI in which an extremely weak plasma discharge is produced to yield the ART fluorescence signal. ART resonantly ionizes the target molecules by REMPI; since REMPI is a highly non-linear optical process, the energy deposition into the surrounding medium is sufficiently small [11]. When a measurement was conducted to quantify the amount of energy deposited into the flow, the scientific grade, high-sensitivity laser power meter used was unable to detect any change in output energy from pre-focal spot to post-focal spot of a 300mm spherical lens with input wavelength of 287.5nm at 30mj/pulse. To achieve the O<sub>2</sub> ART thermometry, specifically chosen rotational bands of O<sub>2</sub> are excited via focusing a frequency doubled Dye laser with sufficient energy, such that a fluorescence line is generated and imaged. The focused laser energy generates additional ionization of molecular nitrogen by avalanche ionization. The recombination of electrons and molecular nitrogen ions produces emissions of the first negative band  $N_2^+(B^2\Sigma_u^+ - X^2\Sigma_g^+)$ , [12] i.e.,

- 1. (2+1) REMPI for molecular oxygen, producing photoelectrons:  $O_2 + 3hv_{REMPI} \rightarrow O_2^+ + e^-$
- 2. Electron impacted avalanche ionization of molecular nitrogen, producing  $N_2^+$ :  $N_2 + e^- + \hbar \nu \rightarrow N_2^+ + 2e^-$
- 3. The first negative and first positive bands of molecular nitrogen ions,  $N_2^+(B) \to N_2^+(X) + \hbar \nu_{1^-}$  or  $N_2^+ + e^- \to N_2(B) \to N_2(A) + \hbar \nu_{1^+}$

The resulting emissions from the first negative band ( $\Delta v_0$ , ~390nm;  $\Delta v_2$ , ~425nm;  $\Delta v_1$ , ~430nm) of N<sub>2</sub> are captured. Any light outside the band is removed via an optical bandpass filter. The signals are post-processed and the resulting values from the various bands are fed into a Boltzmann relationship that yields a 1D line temperature measurement with a nominal error of ±4%. To the authors knowledge, this novel, groundbreaking technique represents the first demonstrated non-intrusive optical *line thermometry* that does not require flow seeding and is the first new technique of this type since the advent of CARS. The technique is capable of generating up to 6 cm long lines, which give it an unprecedented capability of imaging the thermal gradients present in boundary layers and areas of interest in high-speed test facilities. In this paper, the establishment of technique is described in detail, providing future researchers the fundamental calibration studies of O<sub>2</sub> resonate peak sensitivities, suitable peaks for accurate measurements at various temperatures, and theoretical modeling of the O<sub>2</sub> (2+1) REMPI spectrum.

# III. Experimental Setup 3. 1. Focusing Lens Fused Silica Glass Cell Thermocouple exhaust Beam Dump heater Flow Controller chiller Spectrometer Intensified Camera N<sub>2</sub> Emission Laser -flow 7.

Figure 1: ART calibration study experimental setup

A general rendering for the calibration experiment for O<sub>2</sub> ART is shown in Fig. 1. The second harmonic of an Nd:YAG Laser (Continuum Surelite SL-10) with a pulse width of 8ns, repetition rate of 10 Hz, and 200mJ/pulse lasing energy was used to pump a dye laser (Continuum ND6000) that utilized a mixture of Rhodamine 590 and Rhodamine 610 to produce lasing light around 574nm (0.02 cm<sup>-1</sup> linewidth). The dye laser was frequency doubled to generate ultraviolet (UV) beam using an auto-tracker (Continuum UVT-1) to maintain a constant conversion efficiency from the frequency doubling crystal. The UV beam had energy of ~10 mJ/pulse from 285 to 287.5nm. The UV beam was focused using a fused-silica spherical lens with focal length of 150mm, which generated a 1-inch long fluorescence line. The line was centered in a cylindrical, fused-silica glass cell. The emission spectra were collected via two +100mm spherical fused silica lenses that served to focus the light onto the slit of a spectrometer (Princeton Instruments, 600gr/mm blazed at 500nm) with a 50µm slit width. The spectrum was imaged via an intensified scientific camera (PI-MAX4 1024f) with the sensor size of 1024x1024 pixels. To avoid local heating and maintain a uniform species number density in the area of interest, a constant flow of air was provided to the cell at a rate of 0-50 L/min via an electronic flow controller (OMEGA). Depending on the desired calibration temperature the air passed through either a flow heater (OMEGA) or through a custom-built flow-chiller to achieve temperatures ranging from 180 to 470 Kelvin. The air temperature was monitored inside the cell using a k-type thermocouple (OMEGA) that was epoxied into a port to allow for direct measurement.

## IV. Theoretical and Experimental Results

# A. ART from O2 REMPI Theory

Comparison of REMPI spectra of air by coherent microwave scattering (Radar REMPI) [13] and peak fluorescence near 390nm at atmospheric pressure and room temperature has shown great similarity [14]. The intensity of nitrogen fluorescence near 390nm closely follows the (2+1) REMPI excitation of molecular oxygen. The spectra from both microwave scattering and  $N_2$  fluorescence show great similarity, showing all major ro-vibrational lines of molecular oxygen. The prominent band representing 2+1 REMPI with the initial 2-photon transition  $O_2(C^3\Pi \text{ (v=2)} \leftarrow X^3\Sigma \text{ (v'=0)})$  lies between 285-289nm.

Shown in figure 2 is the theoretical REMPI O<sub>2</sub> spectrum at 180, 293, and 473 Kelvin. The model used for calculating the theoretical spectrum is described in detail in previous publications [13, 14]. The model indicates that as the temperature rises from 180K, population distributions shift towards higher rotational states, resulting in increased structure in the spectrum. Thus, the peaks that could be suitable contenders for O<sub>2</sub> ART change depending on the temperature of the test medium. Furthermore, a more in-depth look at the model reveals that certain peaks signal does not vary as a function of temperature (i.e., band heads), these will be avoided as suitable points of interest.

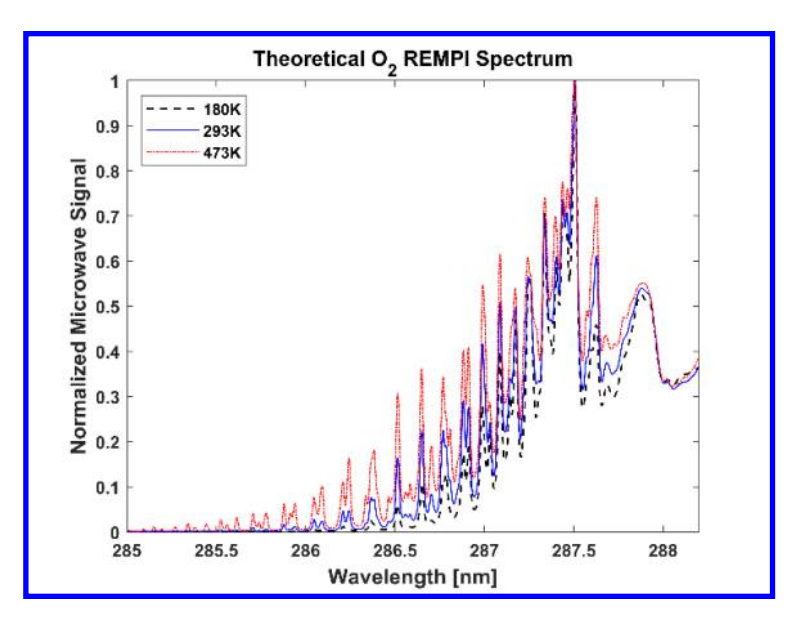


Figure 2: Normalized theoretical O<sub>2</sub> REMPI spectra for 180, 293, 473K

The REMPI structure of  $O_2$  is described in detail in previous literature [15, 16]. A brief summary is shown as the following. The ground state,  $O_2(X^2\Sigma)$ , can be best described as Hund's case (b), in which the splitting due to  $\Sigma' = -1$ , 0, and 1 lead to the hyperfine structure in the ground state, which has been de-noted as  $F_1$ ,  $F_2$ , and  $F_3$ , respectively. The excited state of  $O_2$ ,  $O_2(C^3\Pi)$  can be best described as Hund's case (a), in which  $\Omega$  takes the values 0, 1, 2 respectively. The  $\Omega$  values lead to the hyperfine structure in the C state, which has been denoted as  $S_1$ ,  $S_2$ , and  $S_3$ , respectively. The focus of this study is the two-photon transition line strength  $T_{f,g}^{(2)}$  between the excited state  $C^3\Pi$  and the ground state  $X^3\Sigma$  of their respective Hund's cases and has been modeled in literature [16] and expressed by Equ. 1.

$$T_{f,g}^{(2)} = \sum_{k=0,2} \frac{\left|\beta_k^{(2)}\right|^2}{2k+1} (2J+1)(2J'+1)(2N'+1) \begin{bmatrix} J' & S & N' \\ \Lambda' + \Sigma & -\Sigma & -\Lambda' \end{bmatrix}^2 \begin{bmatrix} J & k & J' \\ \Omega & -\Delta\Lambda & -\Lambda' - \Sigma \end{bmatrix}^2$$
(1)

where, primed parameters are for the ground state of  $X^3\Sigma$  and unprimed parameters are for the excited state of  $C^3\Pi$ .

A previous study of the calculated rotational strengths of the  $S_{21}$  branch transitions based on Eq. 1. was used to identify wavelengths of interest to excite the rotational state of  $O_2$ . Shown in Table 1, are the selected wavelengths that were used to study the fluorescence signal of  $N_2$  and ultimately recover the thermal properties of a 1D line. These wavelengths were chosen due to population distributions being relevant across the selected range at all calibration temperatures.

Table 1: Selected Rotational Lines of S21 for Temperature Measurements

Wavelength	J'	$G_1$	$T_{f,g}^{(2)}$	
nm		cm <sup>-1</sup>		
286.40	21	664.15	12.73	
286.51	19	546.62	11.72	
286.65	17	440.49	10.72	
286.78	15	345.79	9.72	
286.88	13	262.54	8.71	
286.99	11	190.74	7.70	
287.09	9	130.42	6.69	
287.18	7	81.57	5.66	
587.26	5	44.20	4.62	
287.34	3	18.33	3.50	

The values in Table 1, are good for temperatures below 700 kelvin.[14] Using the values from Table 1, the theoretical resultant fluorescence from the two-photon transition from state g to f can be shown by Equ. 2.

$$I_{\lambda_n} \propto N_0 \cdot T_{f_n, g_n}^2 I^2 \cdot exp(-E_{g_n}/k_B T)$$
 (2)

By rearranging Equ. 2. to produce a more useful form in Equ. 3. Where the fluorescence from the selected peaks are termed  $I_{L_n}$ , with n-subscript is typically termed 1-4 and denotes the specific wavelength fluorescence intensity. Four peaks will be selected for each air calibration temperature and a linear fit will be applied to the four signals that result equation 3, using those peak intensities. The resulting fit characteristics, such as  $R^2$  and given temperature will determine which 4 peaks and resultant wavelengths are used.

$$Signal = \log\left(\frac{I_{\Lambda_n}}{T_{f_n,g_n}^2}\right) \tag{3}$$

By taking the signal value from Eq.4 and applying a linear fit to the four selected signals, the slope of the fit will be used to approximate the local rotational temperature in the medium; which is given by Eq.4

$$T_{fit} \propto 1/signal \cdot k_R$$
 (4)

#### **B.** Calibration Experiments for ART

To establish which peaks were most suitable for thermal fits at various conditions, a calibration study was conducted at 180, 233, 293, 367, and 460 Kelvin in a gas cell. Standard air was used as the working gas, and flown at a rate of 42 L/min to ensure the gas molecules in the cell ionized via ART was evacuated and replaced between laser pulses. This was done to avoid localized heating and fluorescence saturation of the gas molecules. Additionally, all fluorescence signals are a 20-image average. This was to minimize shot-to-shot laser fluctuations and background scattering. The use of the spectrometer allowed for discrete analysis of the first negative band of  $N_2^+$ , and each peak as well as the summation of the signals were studied for temperature dependence. Figure 3 shows the  $N_2$  fluorescence spectrum from 287.28nm excitation at standard pressure and the aforementioned temperatures.

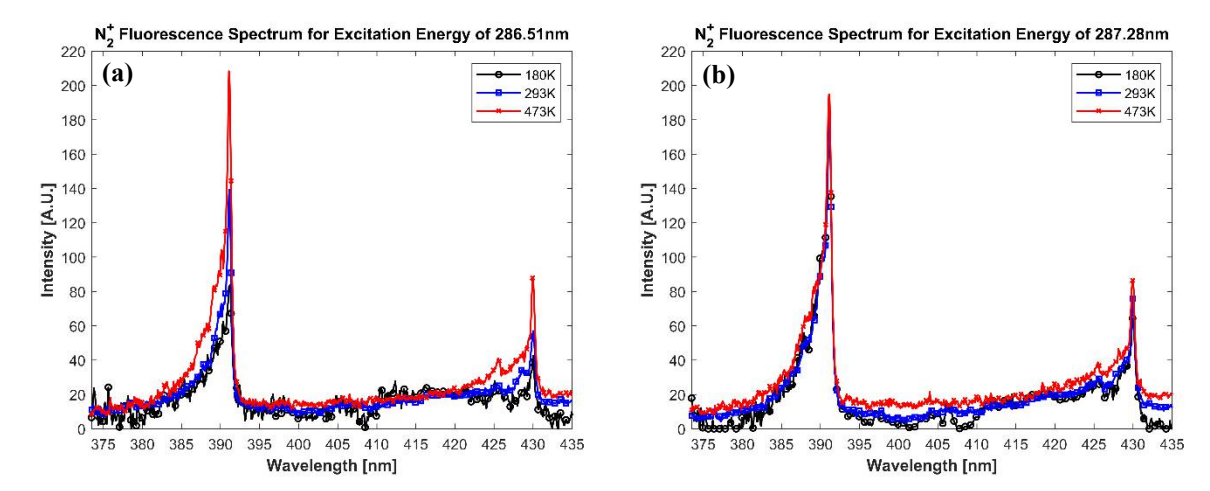


Figure 3: Normalized N<sub>2</sub><sup>+</sup> fluorescence spectrum from (a) 286.90nm and (b) 287.28nm excitation energy.

Figure 3 shows the importance of wavelength selection for excitation, since ART and REMPI are a non-linear processes, different resonant wavelengths have varying degrees of effects. As seen in Fig.3 when standard air is excited with 286.51nm laser beam, the resonant energy is highly dependent on the gas temperature while, 287.28nm excitation results in far less thermal variation. Additionally, in Fig.3 (a), it is clear that as the gas temperature rises, the population distribution trends towards higher states, thus there is an increase in emission intensity in the first negative bands ( $v_2$ , 425nm and  $v_1$ , 430nm) of  $N_2$ . For the calibration study, spectrums similar to the ones in Fig.3 were acquired for all wavelengths listed in Table.1. and at all the aforementioned temperature ranges. To ensure high SNR and adequate spectrum resolutions, each image was background subtracted and collected with 200 accumulated on-chip exposures. The intensity value was found by integrating under each emission band for  $N_2$ . Care was taken to only include signal in the integration and excluding the background contribution. Signal values for 390, 425, and 430nm were studied and found that all emission peaks were capable of supporting ART. For further simplification, integration was performed under the full FOV of the spectrum for the spectrometer. These were then processed using the aforementioned equations, from there 4 peaks were identified that resulted in the best fit; the results are shown in Fig.4.

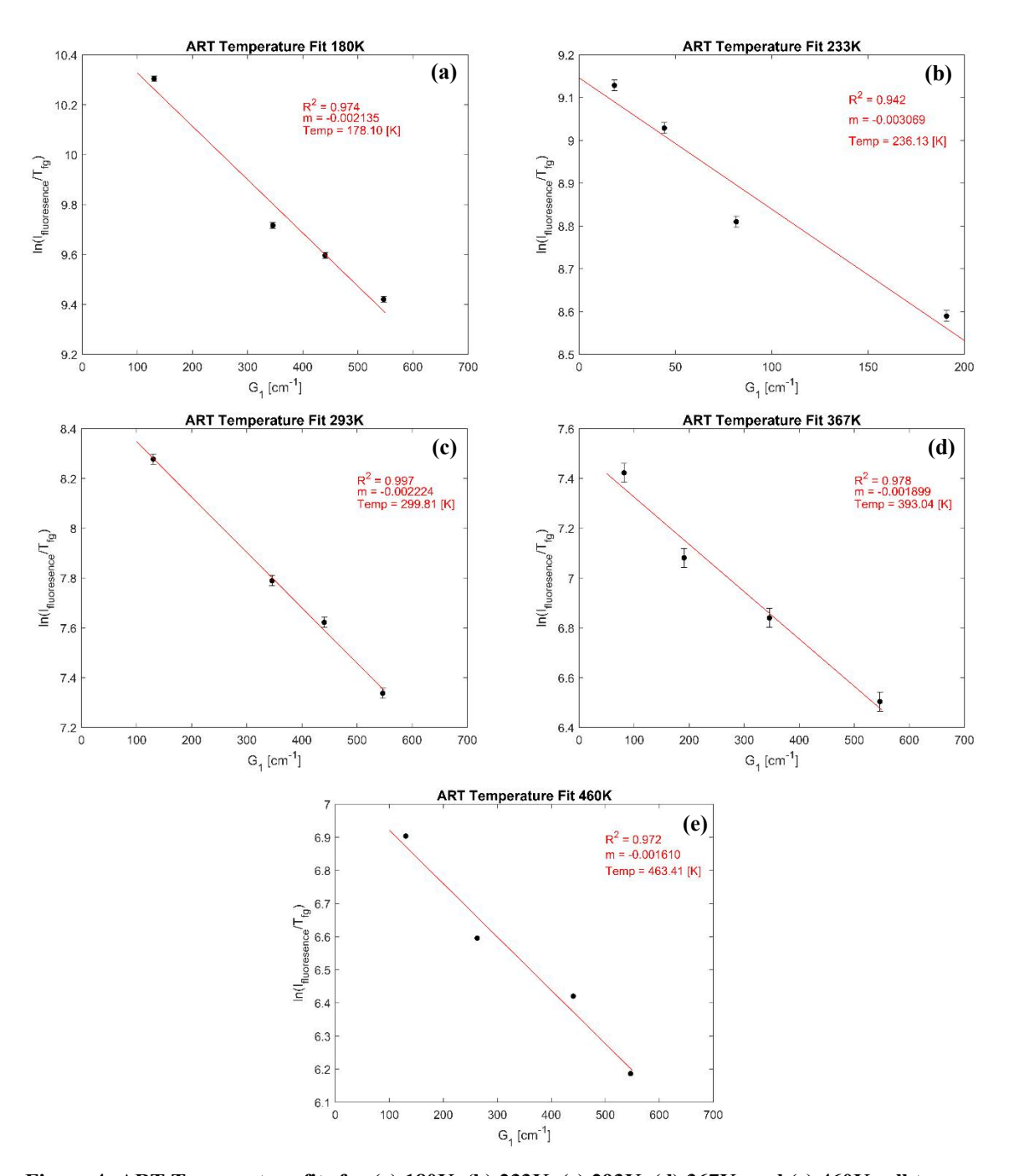


Figure 4: ART Temperature fits for (a) 180K, (b) 233K, (c) 293K, (d) 367K, and (e) 460K cell temps.

Figure 4 is the Boltzmann plot to determine the temperature sensitivities for various peaks. It indicates that through proper peak selection, ART is capable of resolving temperature measurements with ( $\pm 10$ K) accuracy. Peak selections, actual and predicted gas temperatures, and measurement error are detailed in Table2. Based on equation (3) and (4), the x-axis of the Boltzmann plot is the energy of the rotational levels at the ground state,  $E_g$  from Table 1, and the y-axis is a log plot of the relative value of peaks in the experimental ART spectrum scaled by the rotational line strength, ln ( $I_{fluorescence}/T_{fg}$ ). Linear fitted lines are plotted for every measurement. At room temperature, the slope of the Boltzmann line gives a rotational temperature of 299K with an uncertainty of about 3%. At elevated temperatures, the Boltzmann plots give 463K for a furnace temperature of  $T_f = 460$ K with an uncertainty of 3%. Similar measurements show 178K for  $T_f = 180$ K and 236 K for  $T_f = 233$  K. The uncertainties are around 3-6%.

Table 2: Summary of ART parameters for temperature determination

Identified Peaks			Act. Temp.	Meas. Temp	Error	
nm	nm	nm	nm	K	K	%
286.98	287.15	287.28	287.33	180	178	1.11
286.98	287.15	287.28	287.33	233	236	1.29
286.51	286.67	286.79	287.07	293	299	2.05
286.51	286.79	286.98	287.15	367	381	3.81
286.51	286.67	286.90	287.07	460	463	0.65

Table 2. indicates that peak selection is critical for successful modeling of temperature that yields high accurate solutions to ART. It is shown, as temperature decreases, the resonant wavelengths selection trends towards lower energy frequencies. One would expect this, as temperature decreases less structure is apparent in the REMPI spectrum.

#### **V.Conclusion**

In this paper, a new non-intrusive thermometry technique is proposed and validated through a detailed calibration study. By weakly ionizing a medium gas that contains oxygen molecules, ART utilizes resonant wavelengths to selective excite  $O_2$  rotational bands. Through avalanche ionization process,  $N_2$  is thus weakly ionized, producing spectra emissions in the visible region from 395-430nm. The emissions have been shown to be linearly dependent on temperature, albeit if the correct resonant peaks are used.

ART is capable of resolving temperatures with an accuracy of  $\pm 4\%$  and is capable of forming up to a 6cm long line with the current setup used. It represents a major advancement in non-intrusive, non-seeded thermometry techniques for use in low-enthalpy, highspeed flow environments. ART realizes the first 1D line thermometry, giving unprecedented capabilities for characterizing inherent thermal gradients present in boundary layers and other areas of interest. The calibration study found resonant peaks that should be used for different temperature ranges, also the accuracy of the technique and its potential capability were established. Currently, four shots are necessary to achieve an accurate and repeatable thermometry fit. Future work will focus on expanding  $O_2$  ART capability, focusing on achieving thermal line profiles of an under expanded jet and boundary layer thermal gradient characterization on models in supersonic and hypersonic flow regimes.

# VI. Acknowledgements

This work is supported by University of Tennessee, NSF- 2026242 and DOE.

## VII. References

- Kidd, F. G., Narayanaswamy, V., Danehy, P. M., Inman, J. A., Bathel, B. F., Cabell, K. F., Hass, N., Capriotti, D., Drozda, T. G., and Johansen, C. T. "Characterization of the NASA Langley arc heated scramjet test facility using NO PLIF," 30th AIAA Aerodynamic Measurement Technology and Ground Testing Conference. 2014, p. 2652.
- 2. Dogariu, A., Dogariu, L. E., Smith, M. S., Lafferty, J., and Miles, R. B. "Single shot temperature measurements using coherent anti-Stokes Raman scattering in Mach 14 flow at the Hypervelocity AEDC Tunnel 9," *AIAA Scitech 2019 Forum.* 2019, p. 1089.
- 3. Abram, C., Fond, B., and Beyrau, F. "Temperature measurement techniques for gas and liquid flows using thermographic phosphor tracer particles," *Progress in Energy and Combustion Science* Vol. 64, 2018, pp. 93-156.

doi: 10.1016/j.pecs.2017.09.001

4. Gross, K. P., McKenzie, R. L., and Logan, P. "Measurements of temperature, density, pressure, and their fluctuations in supersonic turbulence using laser-induced fluorescence," *Experiments in Fluids* Vol. 5, No. 6, 1987, pp. 372-380.

## doi: 10.1007/bf00264400

- Miller, V. A., Gamba, M., Mungal, M. G., and Hanson, R. K. "Single-and dual-band collection toluene PLIF thermometry in supersonic flows," *Experiments in fluids* Vol. 54, No. 6, 2013, pp. 1-13.
- Danehy, P., Weisberger, J., Johansen, C., Reese, D., Fahringer, T., Parziale, N., Dedic, C., Estevadeordal, J., and Cruden, B. "Non-intrusive measurement techniques for flow characterization of hypersonic wind tunnels," flow characterization and modeling of hypersonic wind tunnels (NATO Science and Technology Organization Lecture Series STO-AVT 325), NF1676L-31725-Von Karman Institute, Brussels, Belgium, 2018.
- 7. Tolles, W. M., Nibler, J. W., McDonald, J., and Harvey, A. B. "A review of the theory and application of coherent anti-Stokes Raman spectroscopy (CARS)," *Applied Spectroscopy* Vol. 31, No. 4, 1977, pp. 253-271.
- 8. Wu, Y., Zhang, Z., and Adams, S. F. "O2 rotational temperature measurements by coherent microwave scattering from REMPI," *Chemical Physics Letters* Vol. 513, No. 4-6, 2011, pp. 191-194.
- doi: 10.1016/j.cplett.2011.07.092
- 9. Sawyer, J., Wu, Y., Zhang, Z., and Adams, S. F. "O2 rotational temperature measurements in an atmospheric air microdischarge by radar resonance-enhanced multiphoton ionization," *Journal of Applied Physics* Vol. 113, No. 23, 2013, p. 233304.
- doi: 10.1063/1.4811533
- 10. Wu, Y., Gragston, M., Zhang, Z., and Miller, J. D. "Spatially localized, see-through-wall temperature measurements in a flow reactor using radar REMPI," *Optics letters* Vol. 42, No. 1, 2017, pp. 53-56.
- 11. Lambropoulos, P. "Topics on multiphoton processes in atoms," *Advances in atomic and molecular physics* Vol. 12, 1976, pp. 87-164.
- 12. Wu, Y., Gragston, M., and Zhang, Z. "Acoustic detection of resonance-enhanced multiphoton ionization for spatially resolved temperature measurement," *Optics Letters* Vol. 42, No. 17, 2017, pp. 3415-3418.
- doi: 10.1364/OL.42.003415
- 13. Zhang, Z., Shneider, M. N., and Miles, R. B. "Coherent microwave scattering from resonance enhanced multi-photon ionization (radar REMPI): a review," *Plasma Sources Science and Technology* Vol. 30, No. 10, 2021, p. 103001.
- doi: 10.1088/1361-6595/ac2350
- 14. Wu, Y., Zhang, Z., and Adams, S. F. "Temperature sensitivity of molecular oxygen resonant-enhanced multiphoton ionization spectra involving the C 3 Π g intermediate state," *Applied Physics B* Vol. 122, No. 5, 2016, p. 149.
- 15. Wu, Y., Bottom, A., Zhang, Z., Ombrello, T. M., and Katta, V. R. "Direct measurement of methyl radicals in a methane/air flame at atmospheric pressure by radar REMPI," *Optics express* Vol. 19, No. 24, 2011, pp. 23997-24004.
- 16. Wu, Y., Sawyer, J., Zhang, Z., and Adams, S. F. "Flame temperature measurements by radar resonance-enhanced multiphoton ionization of molecular oxygen," *Applied optics* Vol. 51, No. 28, 2012, pp. 6864-6869.